sustainability

MDPI

Article

Enhanced Non-Communication-Based Protection Coordination and Advanced Verification Method Using Fault Impedance in Networked Distribution Systems

Juan Noh [1], Seungjun Gham [1], Myungseok Yoon [1], Wookyu Chae [2], Woohyun Kim [2] and Sungyun Choi [1,*]

[1] School of Electrical Engineering, Korea University, Seoul 02841, Republic of Korea; zuan@korea.ac.kr (J.N.); ghamnamu@korea.ac.kr (S.G.); msyoon0451@korea.ac.kr (M.Y.)
[2] Smart Power Distribution Laboratory, Distribution Planning Group, Korea Electric Power Research Institute, Daejeon 34056, Republic of Korea; microgrid@kepco.co.kr (W.C.); wh.kim@kepco.co.kr (W.K.)
* Correspondence: sungyun@korea.ac.kr

Abstract: In recent years, the networked distribution system (NDS), which is normally connected to the distribution line (DL), was actively studied as the topology of the future distribution system for reasons such as improving supply reliability, improving line utilization, and increasing the capacity of distribution generators (DGs). However, the NDS creates new issues in terms of protection coordination because of its bidirectional power flow and fault current flow. The issues associated with conventional protection schemes in the NDS include malfunction of protective devices due to bi-directional fault currents and failure of protection coordination due to communication failures between protective devices. When applying a conventional protection method in the NDS, the protection schemes become complicated, and there is a risk of protection coordination failure due to communication failure between protective devices. To solve this problem, this paper proposes an effective and innovative non-communication-based protection algorithm for protection coordination in the NDS. The proposed protection algorithm utilizes fault impedance characteristics, which allow not only determination of whether a fault occurred, but also the ability to identify the exact fault point. Therefore, the proposed method is expected to be sustainably utilized and contribute to developing protection schemes and devices in various system topologies and scenarios in the future. Additionally, this paper addresses the overall concept of hardware-in-the-loop simulation (HILS) and directly verifies the proposed protection algorithm using HILS. Therefore, this study establishes a sustainable foundation for future research on protection coordination using HILS.

Keywords: networked distribution system (NDS); protection coordination; protection algorithm; intelligent electronic device (IED); hardware-in-the-loop simulation (HILS)

check for updates

Citation: Noh, J.; Gham, S.; Yoon, M.; Chae, W.; Kim, W.; Choi, S. Enhanced Non-Communication-Based Protection Coordination and Advanced Verification Method Using Fault Impedance in Networked Distribution Systems. *Sustainability* **2023**, *15*, 15593. https://doi.org/10.3390/su152115593

Academic Editors: Hamed Hashemi-Dezaki, Ali Karimi, Hamed Nafisi and Seyed Amir Hosseini

Received: 11 September 2023
Revised: 27 October 2023
Accepted: 30 October 2023
Published: 3 November 2023

Copyright: © 2023 by the authors. Licensee MDPI, Basel, Switzerland. This article is an open access article distributed under the terms and conditions of the Creative Commons Attribution (CC BY) license (https://creativecommons.org/licenses/by/4.0/).

1. Introduction

1.1. Background

Recently, there was an urgent need to develop measures to reduce CO_2 for environmental challenges, with a surge of interest in climate issues [1]. Renewable energy source (RES), as an alternative power source, is a solution to reduce CO_2, which is increasingly connected to the grid [2]. In contrast to this significant environmental advantage, the increasing number of RESs, which is inverter-based distributed generation (IBDG), introduces other issues related to bidirectional power flow, power electronics for distributed generators (DGs) connection, and the uncertainty of power generation capacity by weather. These can lead to new problems in protection coordination, power quality, and reliability, resulting in many challenges in grid planning and operation [3–7]. These problems occur when the hosting capacity (HC) limit is exceeded, so measures to improve HC are required for distribution system operators (DSOs) and DG investors [8]. In [9–11], various solutions to improve HC are proposed.

In recent years, the need for high power supply reliability rapidly increased because large industrial loads such as semiconductor fabrication plants and data centers can suffer huge economic losses due to outages [12–14]. Therefore, an appropriate solution that simultaneously improves the grid's supply reliability and HC is required. To increase HC, line reinforcement and a networked distribution system (NDS) are proposed [15].

By comparing the line reinforcement scheme of the radial distribution system (RDS), the economic analysis proves that it is cost-effective to reconfigure the grid topology to the NDS. As a result, the NDS is a sustainable solution that can not only effectively improve HC, but also provides many benefits from a grid planning and operation perspective, such as improving grid supply reliability and reducing line losses [16].

1.2. Transition in Distribution System Topologies

Figure 1 shows the topology transition from the RDS to the NDS. Since the RDS with the unidirectional flow, power flow analysis, and protection scheme is relatively simple, it has advantages regarding protection methods and equipment costs. However, from a planning and operation perspective, solutions are needed to address various problems mentioned earlier due to HC exceedance and to improve supply reliability, and the NDS can be a solution for this [17]. To introduce the NDS into the real-world power system, it is necessary to analyze the system under various conditions, such as steady-state analysis, fault analysis, and circulating current, in advance.

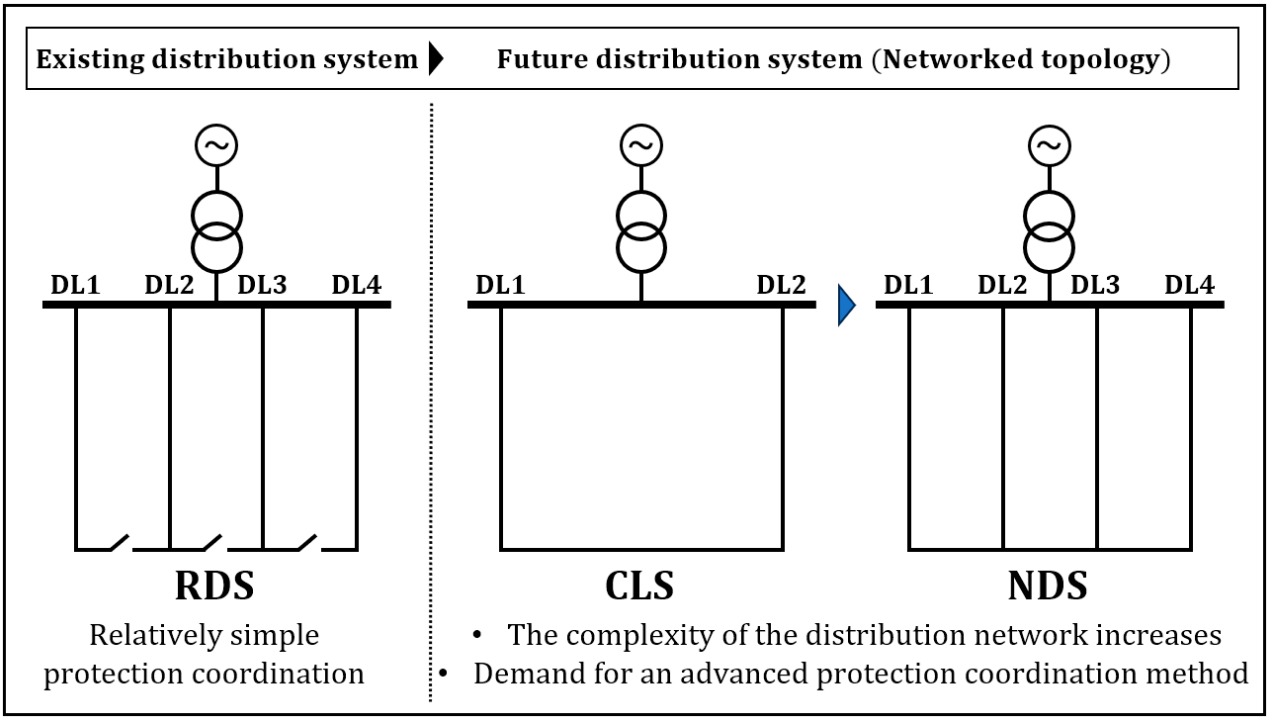


Figure 1. Distribution system topology of RDS, CLS, and NDS.

The closed loop system (CLS) is a simple networked topology with only two distribution line (DL) connections, but it has the disadvantage of keeping the utilization rate of each line below 50% for a single feeder power supply during a fault. Therefore, to increase line utilization and operate the distribution system economically, it is necessary to introduce NDS by increasing the number of connected DLs.

1.3. Protection Coordination in the NDS

An NDS is structurally more complex compared to RDS and CLS, which means that more advanced protection coordination schemes are needed. First of all, it is essential to

secure the operation of the directional overcurrent relay (DOCR) for the bidirectional fault current flows in the NDS [18]. Additionally, to accomplish proper protection in the NDS, innovative protection coordination solutions are required [19–21].

Moreover, the introduction of new devices in the NDS can contribute to advanced protection schemes. When establishing a soft open point (SOP) by linking back-to-back (BTB) converters capable of current control to the switch location of the NDS, the spread of fault can be stably prevented [22]. Additionally, by applying superconducting fault current limiters (SCFCLs) to the NDS, the short-circuit current can be reduced by increasing resistance when a fault occurs. Moreover, when the threshold of SCFCLs are exceeded, the connected line is opened and converted to RDS, so there is an advantage in that the existing protective devices of RDS can be utilized [23].

While the introduction of new devices in the NDS is effective from a protection coordination perspective, it is anticipated that implementing these devices across most NDSs would require substantial equipment costs and time. Therefore, innovative protection coordination schemes are required to effectively introduce an NDS and provide protection coordination at the current system facility level. As a result, this paper proposes a protection algorithm to provide an effective protection coordination scheme and cost-effective solution in the NDS without new devices. Additionally, this paper introduces a robust verification approach utilizing a simulation environment and a real-time simulation environment using hardware-in-the-loop simulation (HILS). Through these methods, the proposed protection formula is directly validated.

1.4. Contributions

This paper introduces fault impedance into the overcurrent relay to enable protection coordination in the NDS. The proposed method is verified in a simulation environment and a real-time simulation environment. The contributions of this study are as follows:

- A protection method for the NDS system with a modified time-current curve (TCC) formula is proposed. Since this method is a communication-less method, there is no concern about protection failures caused by communication errors.
- The proposed method is cost-effective because it does not require new devices such as BTB converters and SCFCLs to provide an advanced protection coordination solution in the NDS.
- The proposed method reflects both features from the TCC of the existing overcurrent relay (OCR) and fault impedance, which ensures faster fault clearance and has less probability of malfunction compared to the conventional OCR-based protection scheme.
- The exact fault location can be inferred from the magnitude of the fault impedance (fault voltage/fault current), which depends on the location. Therefore, it is expected that it can be continuously used in the development of protection schemes and devices in various systems in the future.
- The time-current-impedance (TCI) characteristic takes advantage of the time-current-voltage (TCV) curve and enables more sensitive operation.
- The proposed protection algorithm can be applied to the NDS and RDS systems, making it more versatile.

The organization of this paper is as follows. Section 2 introduces the fault characteristics in the NDS and an overview of HILS. Section 3 describes the proposed TCI-based protection method and protection scheme algorithm. Section 4 verifies the proposed protection method in the simulation and HILS. Finally, Section 5 provides some concluding remarks.

2. Theoretical Background

2.1. Fault Impedance Characteristics

When the fault location is closer to a main power source, more fault current (I_f) flows while the fault voltage (V_f) decreases. By defining this characteristic as TCV, a significant

protection scheme in a NDS with DGs was proposed in [20]. This paper develops the protection scheme using I_f and measured fault impedance (Z_f). The proposed method can take advantage of TCV due to the proportional nature of Z_f and V_f, as shown in Equation (1). In addition, the protection method using Z_f is more sensitive than the voltage characteristic of TCV. For example, suppose the I_f increases by a factor of 5 while the V_f decreases by one-third during fault. Consequently, the resulting Z_f rapidly decreases by a factor of 15, which is the ratio of the V_f to the I_f. This Z_f is used as a factor to reduce the operating time.

$$Z_f = \frac{V_f}{I_f}, \left(Z_f \propto V_f, Z_f \propto 1/I_f\right) \tag{1}$$

Additionally, the magnitudes of the V_f and I_f are determined by the fault location. Therefore, the Z_f, expressed as the ratio of V_f and I_f, differs by the fault location. This means that the exact fault location (Z_f is the minimum point) can be inferred by measuring the characteristic value Z_f of each point, which can improve the selectivity of the protective device.

When a fault occurs in the system, V_f is minimized due to the voltage drop at the fault point, and I_f becomes a maximum value at the fault line. In other words, according to the proportional/inverse relationship between the system fault characteristics and Equation (1), Z_f forms a V-shaped curve with a minimum value at the fault point. Therefore, the magnitude of Z_f decreases as it gets closer to the fault point, which is why Z_f appears in the form of a V-curve, as shown in Figure 2. However, the magnitude of Z_f depends on whether the I_f flows from the source side or the load side. This is because, in the NDS, the magnitude of the source-side I_f is larger than the load side, resulting in a smaller source-side Z_f slope.

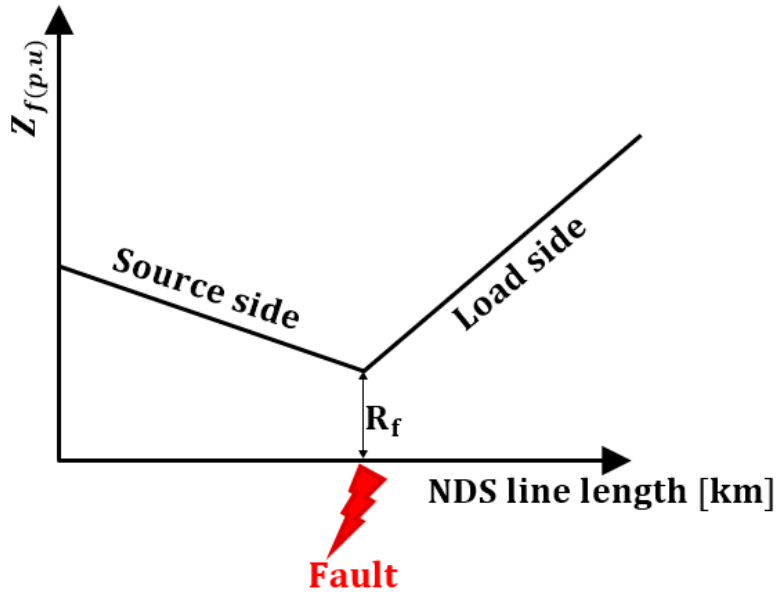


Figure 2. Fault impedance characteristics in the NDS.

2.2. Fault Current Analysis and Direction Detection

Figure 3 shows the characteristics of the I_f during a fault in the NDS and RDS. When a fault occurs, only the I_f on the source side flows in RDS. On the other hand, in the NDS, not only the I_f on the source side, but also the I_f flows on the load side by the connected DL. To remove this bidirectional I_f, both circuit breakers (CB_s on the source side and CB_l on the load side) must operate in Figure 2. For this purpose, based on the polarity of the CT, the protection logic is triggered only when it matches the direction of the I_f.

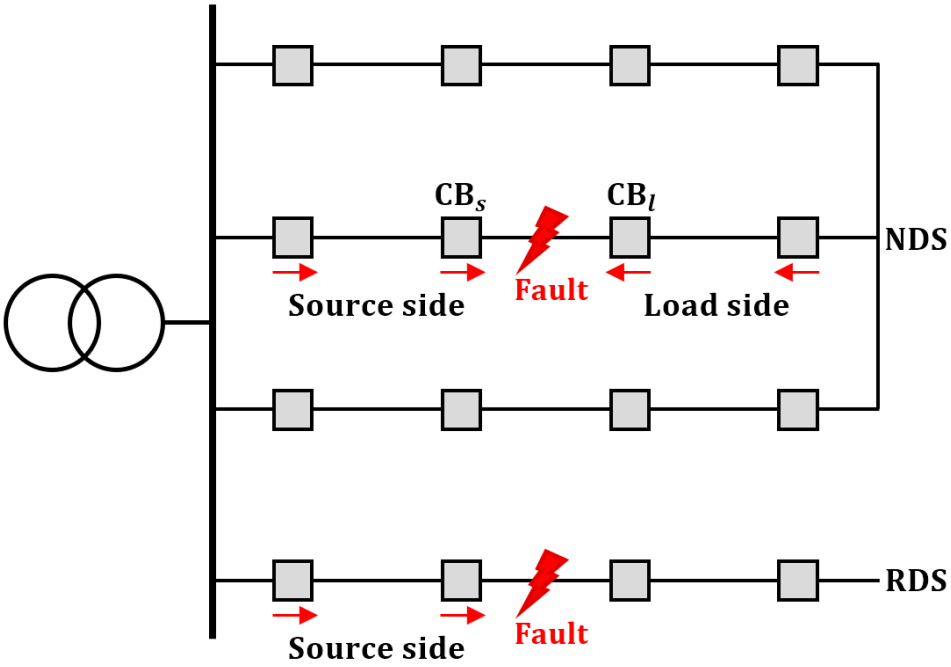


Figure 3. Fault current characteristics in the RDS and NDS.

In general, the direction detection method depends on the type of fault, i.e., the fault detection formula is applied separately for ground faults and phase faults. Equations (2) and (3) show the direction detection formulas of the I_f, respectively, where the nomenclatures are defined in Table 1. $D_0\left(I_f\right)$ is directional detection for the ground fault, and $D_1\left(I_f\right)$ for the short circuit fault. The maximum torque angle (MTA) from the direction detection formula below means the angle to set so that the sensitivity of the protective device to the I_f is maximized in consideration of the line impedance. The operating characteristics of the directional protective devices considering MTA are shown in Figure 4 [24].

$$D_0\left(I_f\right) = cos\left(\angle V_0 - 180^\circ - \angle I_0 - MTA(20^\circ)\right) \tag{2}$$

$$D_1\left(I_f\right) = cos\left(\angle V_1 - \angle I_1 - MTA(60^\circ)\right) \tag{3}$$

Table 1. The nomenclature used in Equations (2) and (3).

Symbol	Description
$D_0\left(I_f\right)$	Function for zero-sequence direction detection
V_0	Measured zero-sequence voltage
I_0	Measured zero-sequence current
$D_1\left(I_f\right)$	Function for positive-sequence direction detection
V_1	Measured positive-sequence voltage
I_1	Measured positive-sequence current

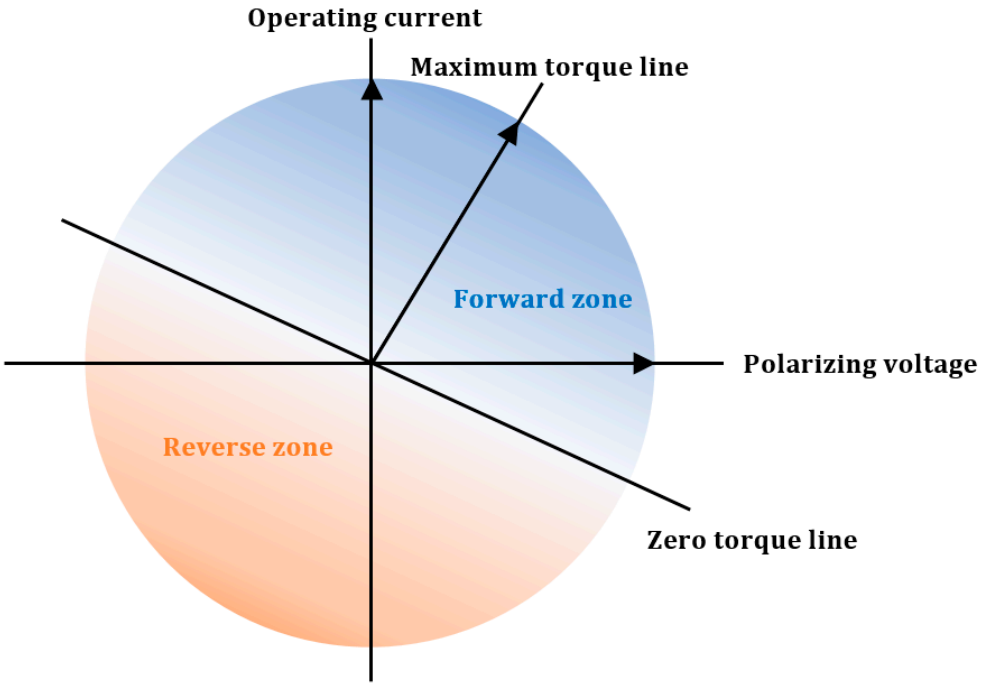


Figure 4. DOCR characteristics according to maximum torque angle.

2.3. Overview of Protection Coordination Using HILS

Recently, grid protection schemes became more complex due to the increasing DGs and the NDS structure that is currently being studied. Therefore, not only advanced protection algorithms are required, but also an efficient protection coordination test method is required [25]. Therefore, this paper proposes a TCI curve-based protection algorithm and a real-time simulation environment-based protection coordination test using HILS. For the protection coordination test, simulation is conducted based on the HILS environment consisting of a Target PC (real-time simulator), algorithms, and firmware updateable test protective hardware known as an intelligent electronic device (IED).

A comparison of the traditional protection coordination test and one using HILS is illustrated in Figure 5. The conventional test environment is costly and time-consuming because a protective device (test hardware) must be manufactured for each validation, and the simulation process must be repeated when an issue occurs. On the other hand, the test method utilizing HILS requires initial facility costs, but when an issue occurs in validation, it can quickly resolve the issue through algorithm and firmware updates after identifying the problems in real-time. Therefore, the HILS-based test sequence can bring financial and time benefits.

Figure 6 shows the HILS configuration used in this paper for the protection coordination test. In this paper, simulation was performed using MATLAB/Simulink software 2022b to verify the proposed formula. For the HILS experimental environment, Speedgoat Target PC, and a IO133 terminal board were used, which has excellent interoperability with MATLAB/Simulink. The inputs for IED are as follows: three types of analog output (AO) (i.e., voltage, current, and neutral current), one type of digital output (DO) (i.e., CB status), and one type of digital input (DI) (i.e., CB operation).

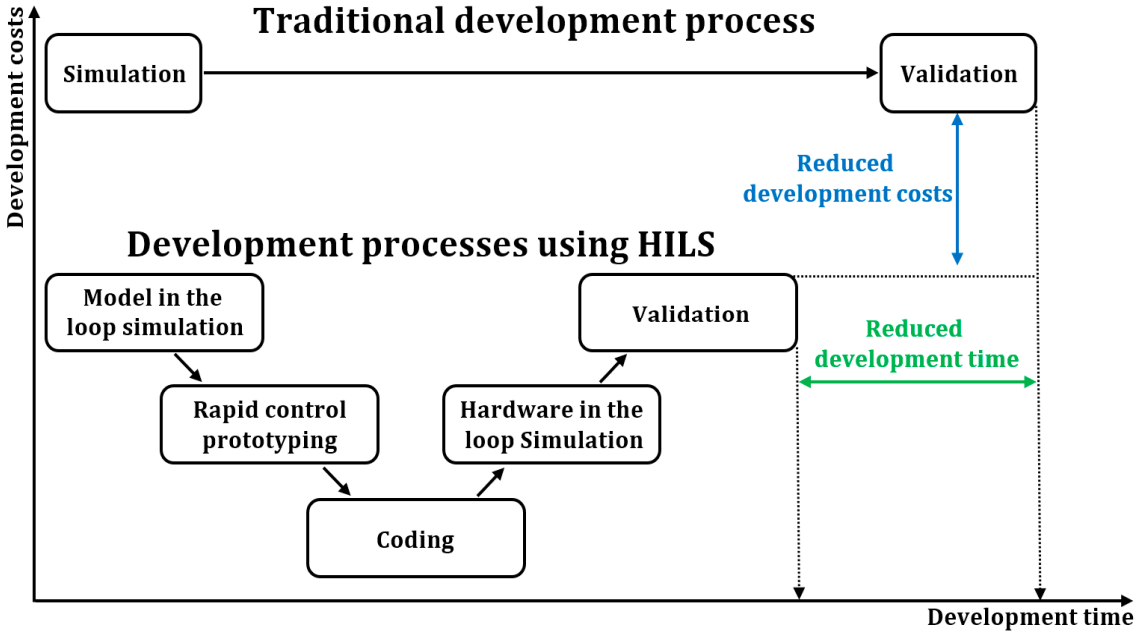


Figure 5. Traditional testing method vs. testing method using HILS.

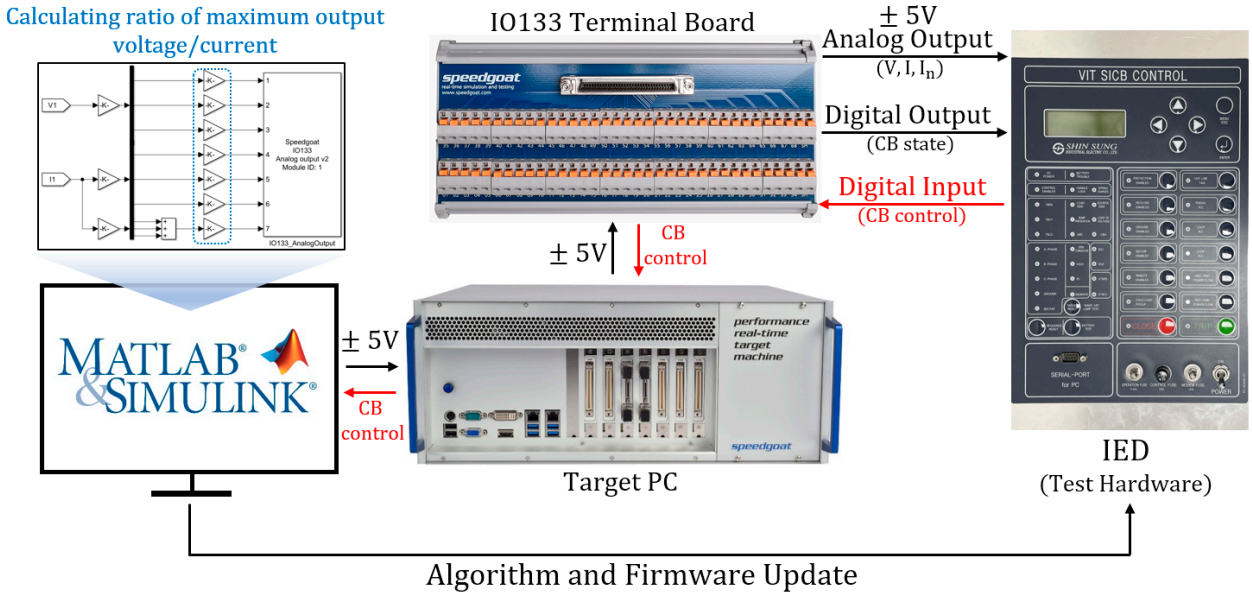


Figure 6. Real-time-based HILS configuration.

When testing using HILS, information about the voltage and current of the test system is input to the hardware as actual voltage through IO. Since the hardware used in this study needs to receive inputs within the scope of ±5 V, the ratio of the maximum output voltage/current was calculated in advance and set to be input into the hardware within ±5 V. Additionally, in a typical HILS process, to recognize current in hardware, it is necessary to convert voltage to current using a power amp. However, the hardware used in this study samples voltage data (magnitude phase) through an internal algorithm and recognizes it as current, so a power amp is not required and provides an advantage in equipment cost. Additionally, since the algorithm can be installed in the IED used in this study through a firmware update, the proposed algorithm was updated and used.

Figure 7 shows the protection coordination test process in the fault scenario with the I/O and circuit breaker model. The scenario is configured with various fault conditions (by changing fault location, fault type, and fault resistance), and the grid data are transmitted to

the IED through the I/O board in the form of AO and DO signals. After the IED determines the fault, the DI signal trips the breaker in the simulation based on the proposed algorithm.

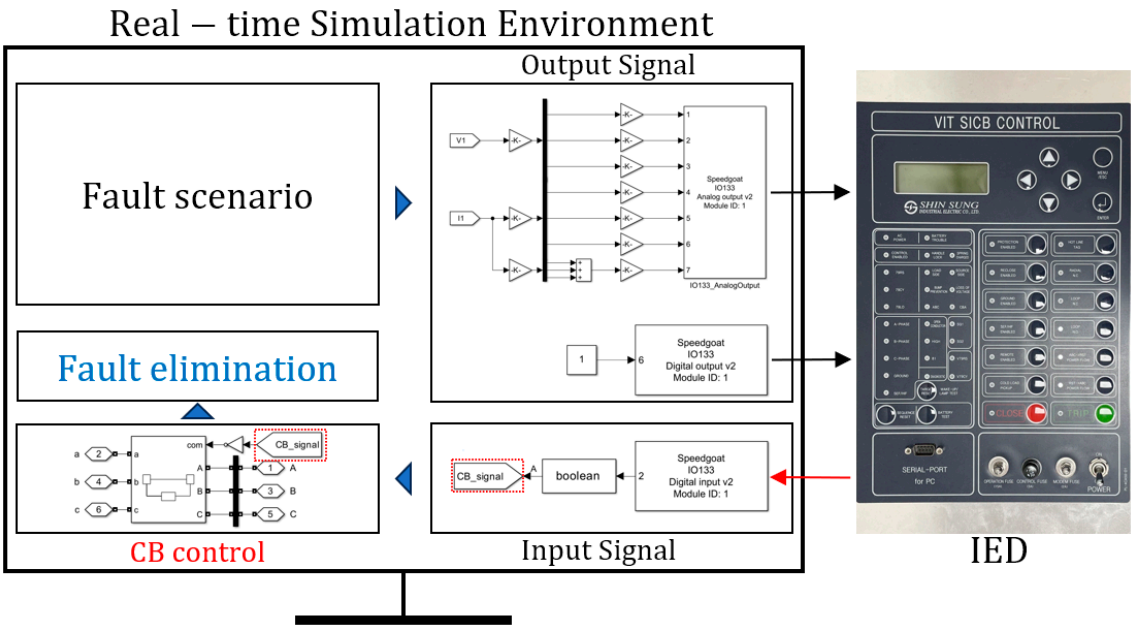


Figure 7. Fault scenario: I/O modeling and operation process.

3. Proposed Method

3.1. Time Current Impedance (TCI) Formula

This paper proposes a formula for protective devices that utilize both I_f and Z_f. The nomenclature of the formula is shown in Table 2, and the proposed protection formula is shown in (4). In this study, the Z_f was used as a per unit value ($Z_{f(p.u)}$) and used as a factor to shorten the operation time of protective devices. The $Z_{f(p.u)}$ value is multiplied by the TCC characteristic of OCR or overcurrent ground relay (OCGR) to determine the protective device operation time. $Z_{f(p.u)}$ decreases closer to the fault point, so the protective device closer to the fault point has the least operating time (t) and is given priority. K is a coefficient that determines 't', which is an adjustable parameter; for example, as K decreases, the protective device operates faster. Consequently, Figure 8 shows an example of the TCI curve proposed in this paper.

Table 2. The nomenclature in Equation (4).

Symbol	Description
t	Relay operating time
TDS	Time dial setting parameter
I_f	Fault current
I_p	Pickup current
$[A, B, C, D]$	Type decision variable of TCC
$Z_{f(p.u)}$	Fault impedance (p.u)

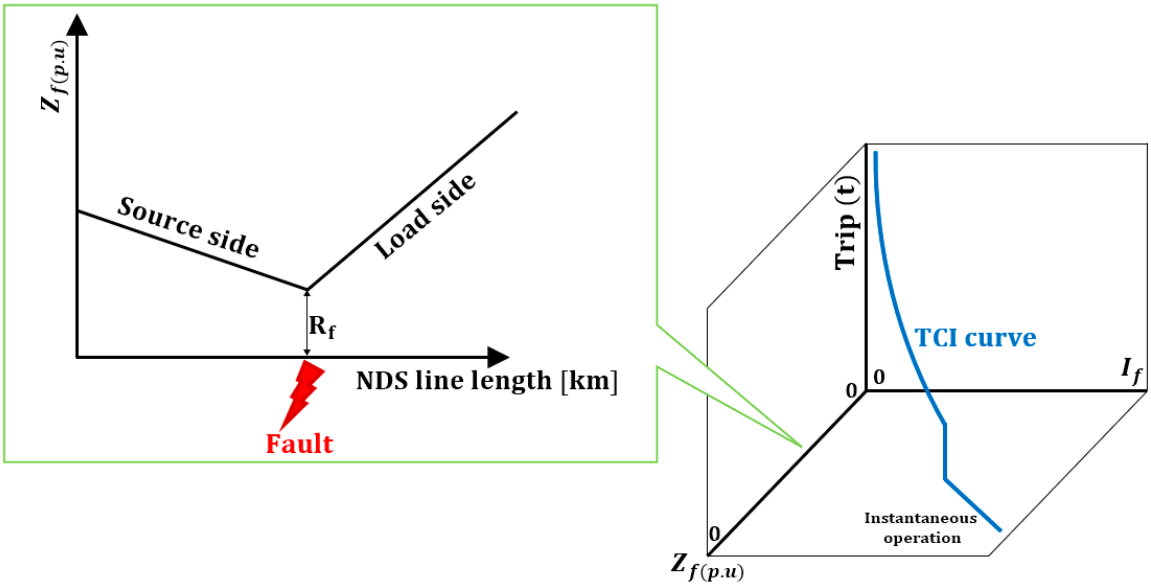


Figure 8. TCI curve characteristics.

In Formula (4), for ground fault detection in the Republic of Korea, the neutral line $I_{p,OCGR}$ is generally set to 70~80 A, and the $I_{p,OCR}$ is set to 400 A when a short circuit occurs. Additionally, since the IEC 60255-3 very inverse (VI) is applied for the TCC setting to determine the protection operating time, the A, B, C, and D in the TCC formula are assumed to be 13.5, 1, 1, and 0, respectively.

$$t = TDS\left(\frac{A}{\left(I_f/I_p\right)^B - C} + D\right)\cdot K\cdot Z_{f(p.u)} \tag{4}$$

However, $Z_{f(p.u)}$ is proportional to the size of the fault resistance (R_f), and there is an issue of $Z_{f(p.u)}$ increasing in the case of a fault with high R_f. Therefore, a method to further advance the proposed protection Formula (4) is required, and the sigmoid function, known as the activation function, was modified and applied additionally. The formula in which the modified sigmoid function is applied to $Z_{f(p.u)}$ is shown in Formula (5), and when this formula is plotted, it appears as shown in Figure 9. Therefore, since $Z\left(Z_{f(p.u)}\right)$ in the formula can remain less than one regardless of the value of the R_f, the operating time of OCR can be guaranteed even in the case of high impedance fault (HIF). As a result, Formula (6) is the final TCI formula proposed in this study after applying modified sigmoid to $Z_{f(p.u)}$.

$$Z\left(Z_{f(p.u)}\right) = \left(\frac{1}{1+e^{-Z_{f(p.u)}}} - \frac{1}{2}\right)\cdot 2 \tag{5}$$

$$t = TDS\left(\frac{A}{\left(I_f/I_p\right)^B - C} + D\right)\cdot K\cdot Z\left(Z_{f(p.u)}\right) \tag{6}$$

3.2. Protection Scheme Algorithm

Figure 10 shows the algorithm flowchart applied to a protective device. In the NDS, the grid voltage and current are always measured by protective devices. To minimize the service outage area during protection coordination in the NDS, the protective devices that are the closest to the fault point should be selectively operated. Therefore, a direction detection algorithm after fault detection is essentially considered. After direction detection,

a proposed TCI is calculated based on the measured voltage and current, and the protective device quickly trips the circuit breaker closest to the point of fault. The high-speed opening of the circuit breaker clears faults quickly and ensures system protection.

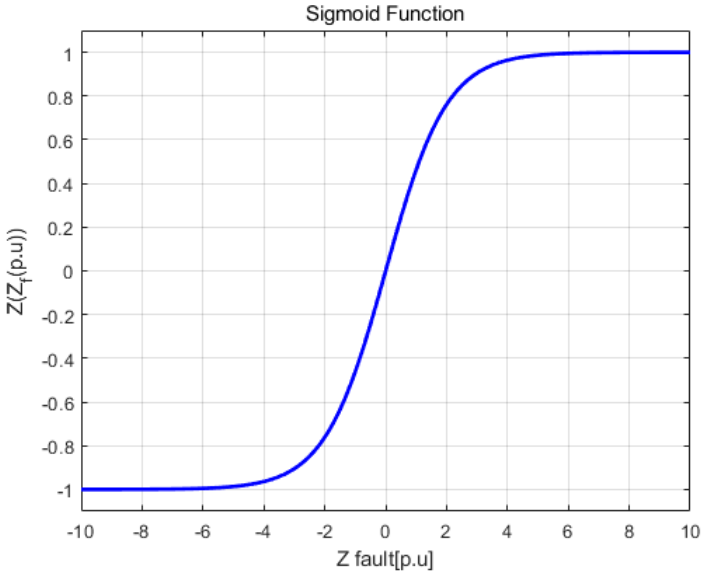


Figure 9. Fault impedance sigmoid characteristic plot.

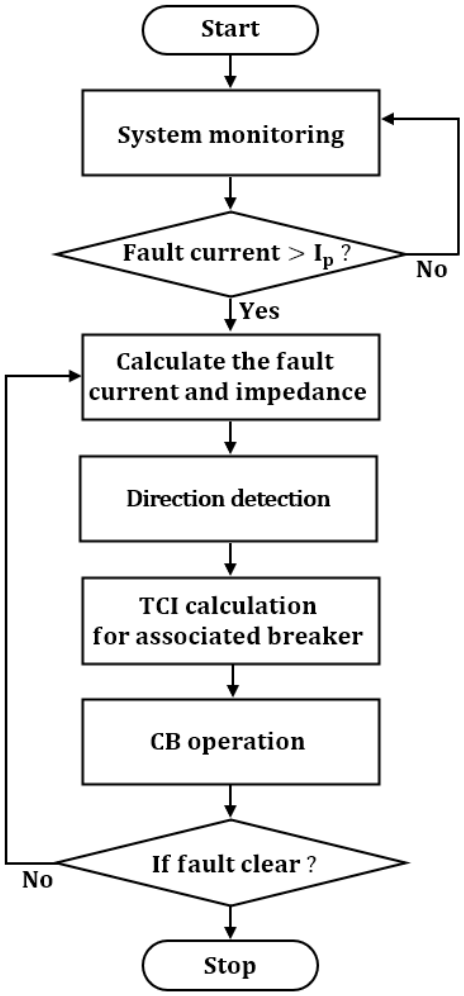


Figure 10. Protection scheme algorithm.

4. Validation

4.1. Simulation Environment

4.1.1. Simulation Environment Setup

It is ideal for the NDS with different load patterns of each DL to be configured by linking DL terminals with the same line length. This is because load sharing is possible for different load patterns on the same line, and the load imbalance can be avoided caused by the voltage differences at the end of the line.

In Section 4, various case studies are conducted to verify the proposed protection algorithm and to check the trend of $Z_{f(p.u)}$. The ideal NDS topology with four distribution lines is illustrated in Figure 11 with the fault points F1 to F8. The proposed protection algorithm is tested by changing the size of the R_f; 0.1, 0.2, 0.3, 0.4, and 0.5 Ω in Case 1 and 0.01, 0.1, and 1 Ω in Case 2. In the fault scenario, the NDS has a different I_f based on the connection at the end of the distribution line. DL1 and DL4 are with one connection; in contrast, DL2 and DL3 are with two. Therefore, to clearly understand the behavior of the proposed protection formula, two types of case studies are conducted.

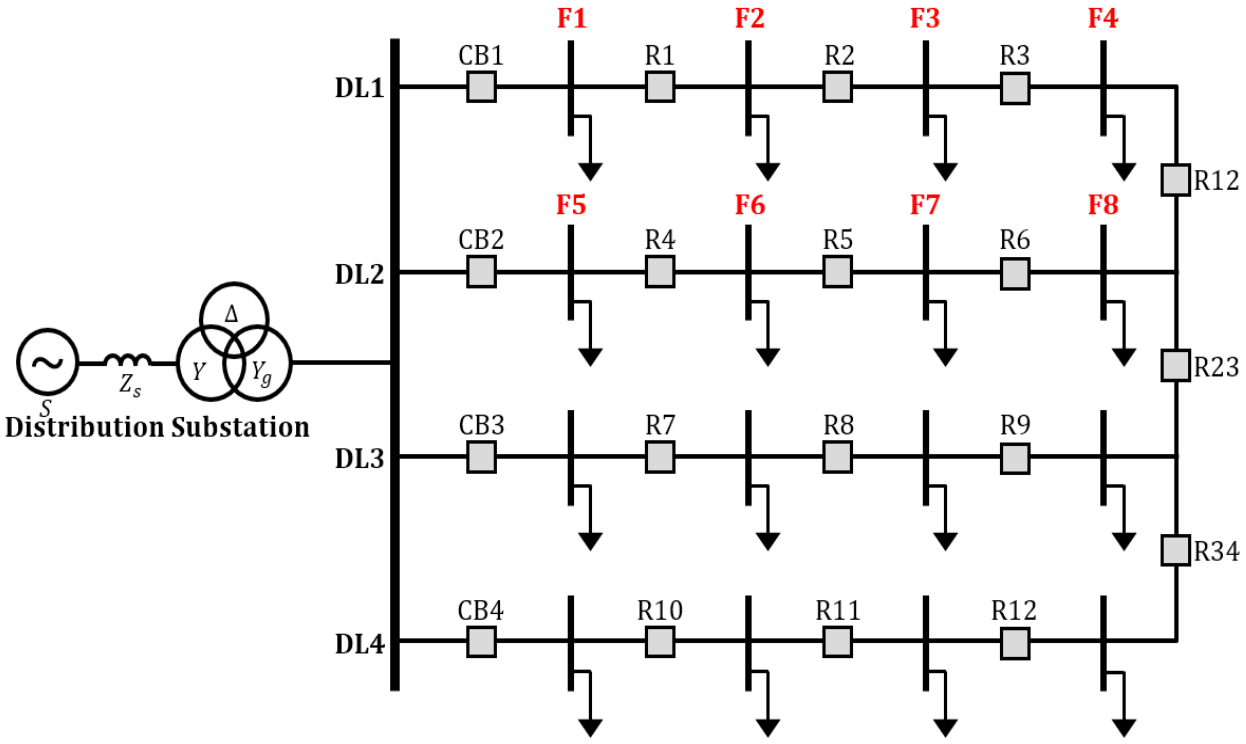


Figure 11. Test NDS systems in Cases 1 and 2.

The test system consists of a voltage source equivalent to the transmission system, a three-winding transformer (154/6.6/22.9 kV), four distribution lines (CNCV 325 mm^2), and loads. The parameters of the system equipment equivalent impedance, section length, and load size of each facility are shown in Tables 3 and 4. To check the tendency of $Z_{f(p.u)}$ during a fault, both the length of the line and the size of the load were uniformly assumed to be 8 km and 2 MW, respectively, and the case with different sizes of R_f was simulated as Case 1. Case 2 is conducted with different load sizes on the same line length and the randomized load size.

Table 3. System equipment equivalent impedance.

Parameter	Value
Source impedance (Z_s)	$Z_1 = Z_2 = 0.00105 + j0.01146$p.u
	$Z_0 = 0.00527 + j0.02900$p.u
Transformer impedance (154/6.6/22.9 kV)	$X_{Tr}^{HM} = j0.14496$p.u
	$X_{Tr}^{ML} = j0.0669$p.u
	$X_{Tr}^{LH} = j0.2538$p.u
CNCV-325 line impedance	$Z_1 = Z_2 = 0.01823 + j0.028222$p.u/km
	$Z_0 = 0.053203 + j0.016495$p.u/km

Table 4. Section length and loads of each DL.

	DL1					**DL2**					**DL3**					**DL4**				
	S - CB1	**CB1 - R1**	**R1 - R2**	**R2 - R3**	**R3 - R12**	**S - CB2**	**CB2 - R4**	**R4 - R5**	**R5 - R6**	**R6 - R12, R23**	**S - CB3**	**CB3 - R7**	**R7 - R8**	**R8 - R9**	**R9 - R23, R34**	**S - CB4**	**CB4 - R10**	**R10 - R11**	**R11 - R12**	**R12 - R34**
Section Length [km]	1	2	2	2	1.5	1	2	2	2	1.5	1	2	2	2	1.5	1	2	2	2	1.5
Case 1 Load [MW]	-	2	2	2	2	-	2	2	2	2	-	2	2	2	2	-	2	2	2	2
Case 2 Load [MW]	-	2.21	2.15	1.62	1.58	-	2.55	1.89	1.56	1.42	-	1.71	1.94	3.11	1.91	-	1.12	1.65	2.62	1.83

4.1.2. Simulation Result and Discussion

In Figure 12, for Case 1, the trend of the measured $Z_{f(p.u)}$ along the line with a single line-to-ground (SLG) fault is applied at the midpoint of the line, fault location F7. The V-shaped graph shows the value of $Z_{f(p.u)}$ as a function of the length. The minimum value of the $Z_{f(p.u)}$, i.e., the vertex of the V-graph, increases according to the magnitude of R_f. When the fault point changes, $Z_{f(p.u)}$ forms a V-shaped curve with a minimum value at each faulted node. In other words, for faults with smaller R_f, the operating time decreases proportionally. As a result, due to the nature of the V-curve, breakers close to the fault point are prioritized, and low impedance faults critical to the grid can be quickly eliminated.

Next, Case 2 simulates the fault situation on the same NDS with different load sizes. The total load sizes were 7.56, 7.42, 8.67, and 7.22 MW connected to lines DL1, DL2, DL3, and DL4, respectively, and the fault scenario was simulated after the load was equalized by DL connection.

Since SLG faults occur most frequently in the system, it was conducted as a fault test case. Additionally, although three-phase short-circuit faults have a relatively low probability of occurrence in real-world power systems, these faults involve extremely high I_f. In other words, the three-phase short-circuit fault was adopted as a severe fault case. Table 5 shows the results of a comparison between the proposed TCI-based breaker operation time and the conventional one in Case 2. In this case, the value of K is assumed as 1. If necessary, the operating time can be adjusted appropriately by adjusting the K value.

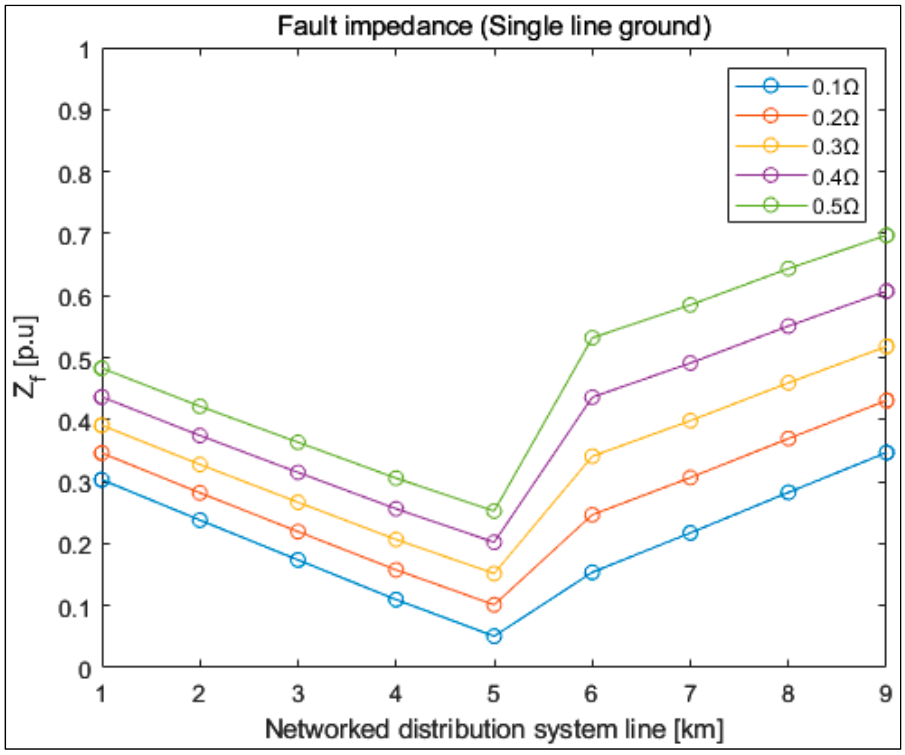


Figure 12. $Z_{f\ (p.u)}$ curve according to change in value of R_f.

In the event of a fault within the power system, the magnitude of the I_f varies depending on the fault location, and typically, the highest I_f flows at the entrance of the feeder (fault location F1, F5). The faster the breaker operation time and minimum service outage, the better, but it is usually specified that the breaker operation time should be within 100 ms based on the entrance of the feeder. In this study, 100 ms is used as an evaluation metric, and exceeding this indicates a negative impact on system reliability. According to the simulation results, when the conventional protection method is applied, the breaker operation time exceeds 100 ms, resulting in negative effects on system reliability. In addition, in the case that R_f= 0.01 Ω, I_f of more than 6~8 kA may flow, which can cause hazardous adverse effects in the grid facilities. On the other hand, the proposed method, regardless of the type of fault and the size of R_f, ensures the operation time of the source-side and load-side breakers is within 100 ms, which means it is a reliable protection scheme for the NDS.

4.2. Real-Time Environment

4.2.1. Simulation Environment Setup

In a real-time environment, based on the Gochang Power Test Center (Gochang PTC) of the Korea Electric Power Corporation (KEPCO), which is used to demonstrate power facilities in Korea as a test center, the NDS is modeled and used as a HILS test system as shown in Figure 13. The numbers in Figure 13 represent the actual multi-circuit breaker numbers of the Gochang PTC. In real-world Gochang PTC, to apply various fault conditions, the artificial fault generator (AFG) is used in the demonstration of protective devices, and the fault situation is simulated where switchgear is in the grid. Therefore, the fault scenario for HILS is also simulated based on the switchgear location. The specific purpose of the fault simulation is shown in Table 6. Figure 14 shows HILS for case studies (Cases 3 and 4).

Table 5. Circuit breaker operation time in Case 2.

	Fault Type	R_f **[Ω]**	**F1**		**F2**		**F3**		**F4**		**F5**		**F6**		**F7**		**F8**	
			Source	**Load**	**Source**	**Load**	**Source**	**Load**	**Source**	**Load**	**Source**	**Load**	**Source**	**Load**	**Source**	**Load**	**Source**	**Load**
Conventional method	AG	0.01	0.102	0.150	0.102	0.204	0.057	0.159	0.081	0.183	0.102	0.147	0.044	0.146	0.061	0.163	0.092	0.138
		0.1	0.102	0.151	0.102	0.204	0.058	0.160	0.083	0.185	0.102	0.148	0.045	0.147	0.062	0.164	0.094	0.140
		1	0.102	0.160	0.122	0.224	0.081	0.183	0.106	0.208	0.102	0.157	0.056	0.158	0.078	0.180	0.121	0.179
	ABC Short	0.01	0.101	0.203	0.102	0.204	0.254	0.356	0.385	0.487	0.101	0.223	0.102	0.204	0.270	0.372	0.443	0.545
		0.1	0.101	0.203	0.102	0.204	0.255	0.357	0.387	0.489	0.102	0.204	0.103	0.205	0.271	0.373	0.445	0.547
		1	0.101	0.333	0.123	0.225	0.272	0.374	0.416	0.518	0.121	0.223	0.124	0.226	0.290	0.392	0.479	0.581
Proposed method	AG	0.01	0.010	0.024	0.013	0.026	0.014	0.027	0.015	0.026	0.010	0.024	0.013	0.026	0.014	0.026	0.015	0.028
		0.1	0.011	0.025	0.013	0.027	0.014	0.027	0.015	0.027	0.011	0.025	0.013	0.026	0.015	0.028	0.016	0.030
		1	0.015	0.031	0.016	0.031	0.026	0.041	0.050	0.064	0.015	0.030	0.017	0.032	0.030	0.045	0.065	0.082
	ABC Short	0.01	0.012	0.026	0.014	0.028	0.014	0.028	0.016	0.029	0.012	0.026	0.014	0.028	0.014	0.027	0.016	0.030
		0.1	0.012	0.026	0.014	0.028	0.015	0.029	0.017	0.030	0.012	0.026	0.014	0.028	0.015	0.028	0.018	0.032
		1	0.014	0.031	0.017	0.034	0.035	0.050	0.075	0.089	0.014	0.031	0.018	0.034	0.040	0.055	0.099	0.117

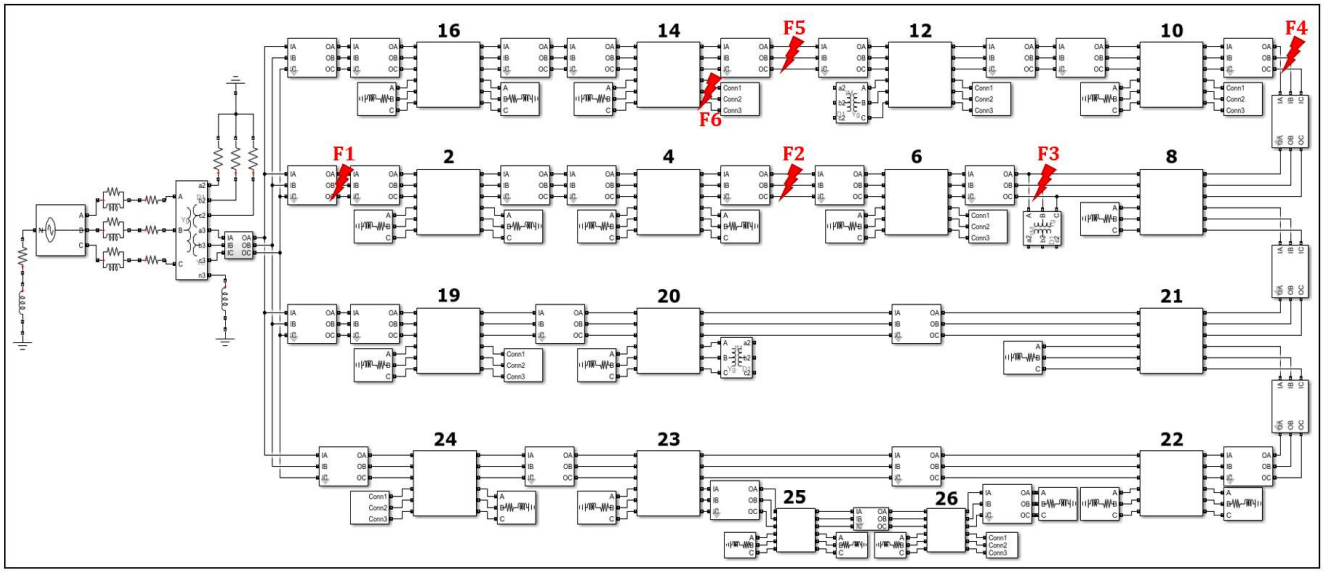


Figure 13. Gochang PTC test system model.

Table 6. Gochang PTC fault scenario.

Fault Number	Fault Test Purpose
F1	Feeder entrance fault scenario
F2	Feeder midpoint fault scenario
F3	DG connection point fault scenario
F4	Feeder terminal interconnection fault scenario
F5	Feeder midpoint fault scenario
F6	Lateral fault scenario

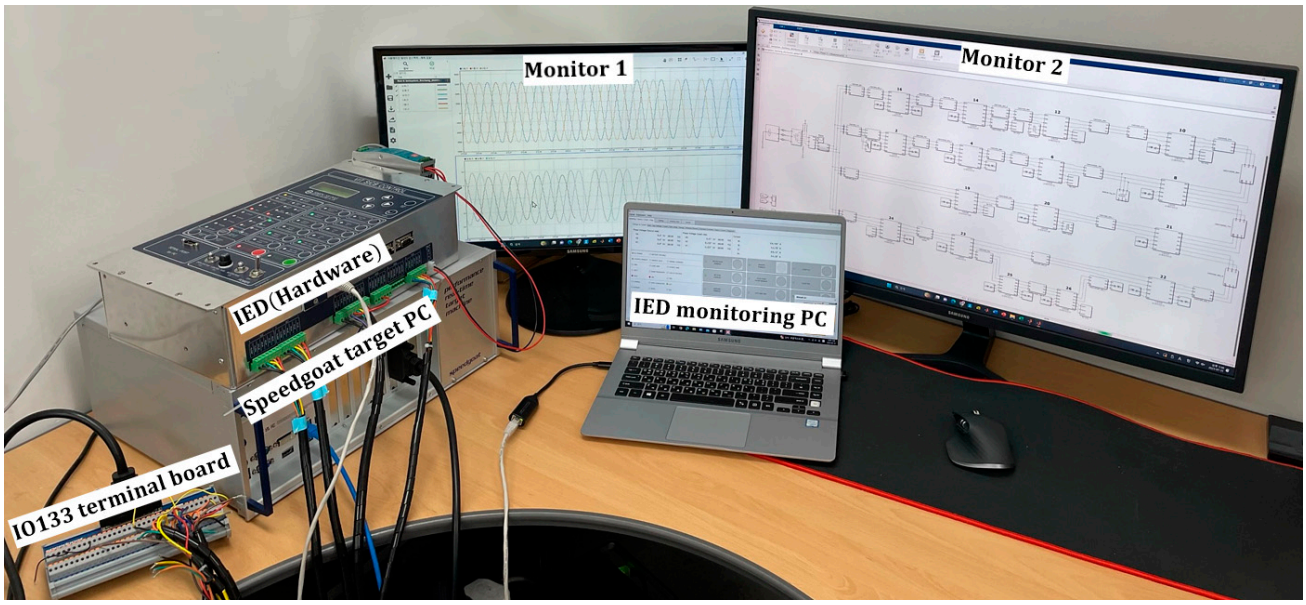


Figure 14. HILS for Cases 3 and 4.

The equivalent impedance of the Gochang PTC is the same as shown in Table 3. The remaining equipment is modeled with the same location and capacity as the Gochang

PTC's actual equipment. Gochang PTC has virtual load units with a 300 kW capacity each (100 kW per phase), which serve as connected loads. Therefore, this case study was conducted with 900, 1200, 600, and 900 kW loads attached to DL1, DL2, DL3, and DL4, respectively. Furthermore, for Case 4, 1-MVA DGs are connected to the lateral of DL1 and DL3, and a 500 kVA DG is connected to the feeder DL2.

Unlike Cases 1 and 2, the Gochang PTC test system model has different line lengths. Table 7 shows the section length of the network and the locations where the load and DGs are connected. In Case 3 (HILS with Gochang PTC-based NDS), the proposed protection algorithm will be verified in the system without DGs. The test system consists of short distribution lines (CNCV 325 mm^2) and is characterized by low line utilization per DL due to small load size. In the simulation environment, the general three-phase breaker component of MATLAB/Simulink is utilized. The breaker component is operated by the signal from the hardware (relay) after determining the fault through the protection algorithm.

The DG is normally interconnected with Yg-D-wound transformers. When a fault occurs in a DG-connected system, a protective device may malfunction, or a protective device may trip at any point. This is because the zero-sequence I_f flows back into the system through the neutral line of the Yg-D-connected transformer. As a result, the magnitude of I_f is attenuated, not reaching the directional determination threshold, which means directional determination failure and breaker inactivity. Therefore, it is necessary to test whether the proposed protection algorithm can operate normally in a DG-connected system, which is configured as Case 4.

4.2.2. HILS Result and Discussion

Figures 15 and 16, respectively, represent the magnitude of the fault current and the circuit breaker operation signal caused by the SLG fault and 3-phase short circuit scenarios at the entrance of DL2 (Fault 1 scenario) in Case 3. In these results, a fault with R_f of 1 Ω is simulated to occur at 0.3 s. The magnitudes of the two peaks of I_f are over 9 kA and 15 kA. Considering that the rated RMS current of the circuit breaker is 12.5kA, it can be seen that a very high I_f flowed. Therefore, it is necessary to clear the fault quickly to protect the grid facilities. According to the proposed algorithm, the circuit breaker was tripped in 0.034 and 0.032 s, respectively. As shown in the graphs below in Figures 15 and 16, respectively, the operation time of the circuit breaker is defined as the time from the fault occurrence (at 0.3 s) to when the output of the circuit breaker control signal changes to 1. Consequently, the fault clearing time includes the fault detection time, fault judgment time, and circuit breaker operation time (the sum of breaker contact opening time and arc extinguishing time), and the fault was cleared within three cycles.

Table 8 presents the results of circuit breaker operation times under fault scenarios for Case 3 and Case 4. For the same reasons as Case 2, simulations are conducted for an SLG fault, and a three-phase short-circuit fault to test protection coordination. The comprehensive analysis of these case studies shows that regardless of the type of fault, the magnitude of R_f, and the location of the fault, the breaker can be tripped within 100 ms in all scenarios, ensuring effective power system protection. Particularly in Case 4, where DG is integrated, the proposed method can prevent the inactivity of nearby circuit breakers at the fault point and mitigate malfunction of circuit breakers unrelated to the fault caused by the zero-sequence current flowing through the neutral line of Yg-D transformers. This prevention is achieved through the characteristics of Z_f, where the circuit breakers closest to the fault point operate first before the operation of unrelated circuit breakers. In summary, the proposed method demonstrates its potential to resolve various issues of protective devices, even in future power distribution systems with an increasing penetration of DGs.

Table 7. Test Gochang PTC parameters (Cases 3 and 4).

	DL1					**DL2**					**DL3**				**DL4**			
	S - CB16	**CB16 - R14**	**R14 - R12**	**R12 - R10**	**R10 - R8**	**S - CB2**	**CB2 - R4**	**R4 - R6**	**R6 - R8**	**R8 - R8, R21**	**S - R19**	**R19 - R20**	**R20 - R21**	**R21 - R8, R22**	**S - R24**	**R24 - R23**	**R23 - R22**	**R22 - R21**
Section Length [km]	0.077	0.049	0.085	0.086	0.077	0.061	0.065	0.055	0.018	0.077 0.017	0.03	0.04	0.04	0.017 0.08	0.03	0.04	0.04	0.08
Case 3 Load [kW]	-	-	300	300	300	-	300	300	600	-	-	300	300	-	300	-	600	-
Case 4 DG location [MVA]	-	-	1	-	-	-	-	-	0.5	-	-	-	1	-	-	-	-	-

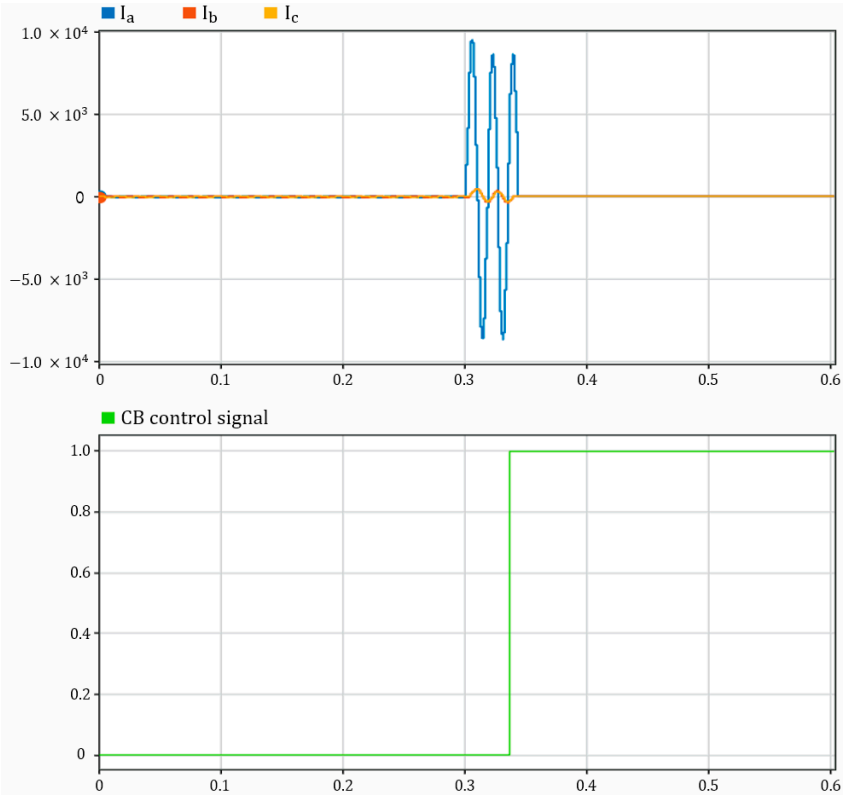


Figure 15. Simulation results in the HILS test environment when a SLG fault occurs (top: fault current, bottom: circuit breaker control signal).

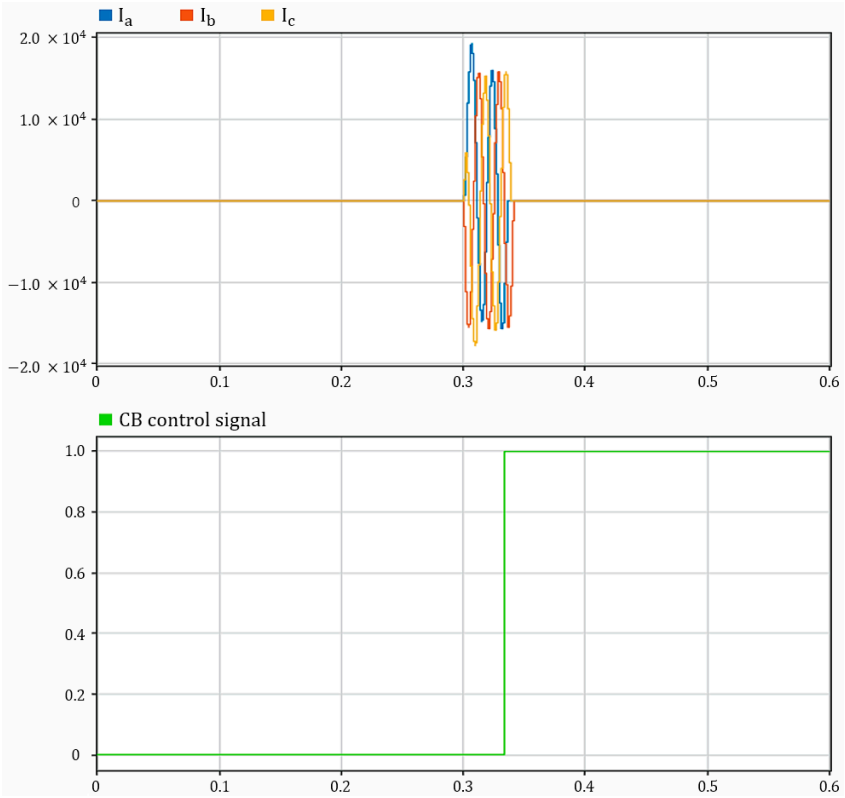


Figure 16. Simulation results in the HILS test environment when a three-phase short circuit occurs (top: fault current, bottom: circuit breaker control signal).

Table 8. Circuit breaker operation time in Cases 3 and 4.

	Fault Type	R_f [Ω]	F1		F2		F3		F4		F5		F6	
			Source	Load	Source	Load	Source	Load	Source	Load	Source	Load	Source	Load
Normal load condition	AG	0.01	0.024	0.054	0.028	0.057	0.033	0.068	0.033	0.069	0.031	0.064	0.030	-
		0.1	0.025	0.056	0.033	0.060	0.036	0.077	0.041	0.087	0.032	0.067	0.031	-
		1	0.034	0.067	0.035	0.063	0.047	0.108	0.052	0.097	0.046	0.077	0.033	-
	ABC Short	0.01	0.030	0.060	0.034	0.065	0.029	0.058	0.032	0.066	0.033	0.063	0.028	-
		0.1	0.032	0.060	0.034	0.066	0.035	0.074	0.034	0.067	0.033	0.064	0.03	-
		1	0.032	0.064	0.038	0.067	0.066	0.165	0.064	0.118	0.033	0.064	0.031	-
DG connected condition	AG	0.01	0.033	0.06	0.032	0.062	0.035	0.071	0.036	0.072	0.031	0.061	0.030	-
		0.1	0.033	0.06	0.033	0.064	0.046	0.083	0.037	0.082	0.031	0.061	0.030	-
		1	0.034	0.065	0.039	0.075	0.052	0.113	0.044	0.088	0.044	0.072	0.031	-
	ABC Short	0.01	0.030	0.058	0.030	0.060	0.034	0.064	0.03	0.062	0.029	0.060	0.030	-
		0.1	0.030	0.059	0.034	0.067	0.035	0.074	0.033	0.068	0.032	0.061	0.030	-
		1	0.034	0.066	0.038	0.070	0.065	0.165	0.061	0.112	0.033	0.064	0.031	-

5. Conclusions

Recently, the NDS was actively researched as a solution for HC and reliability enhancement in distribution systems. However, in the NDS, new protection coordination issues arise due to bidirectional fault currents. Additionally, conventional TCC protection methods only have a fault current criterion for determining a fault, so a more sophisticated fault identification method is needed to improve system reliability.

Therefore, this paper proposes a novel protection method based on the TCC protection formula of overcurrent relays and fault impedance characteristics for protection coordination in the NDS. When a fault occurs in the system, the fault impedance magnitude varies at different network points, so the exact location of the fault can be inferred, and the breaker closest to the fault can be selectively operated to minimize the fault section and improve reliability. In addition, this method operates based on non-communication, eliminating the concern of malfunctions caused by communication errors, and it can also be utilized in RDS, so it has the advantage of a wide range of applications. Moreover, the proposed method offers advanced protection solutions even without new devices, so it has advantages in terms of cost-effectiveness.

As a result of verifying the proposed protection method through a case study, it is shown that the fault clearing time can be significantly reduced compared to conventional overcurrent relays. Additionally, both circuit breakers at the entrance of the DL trip within 100 ms regardless of fault current or fault resistance, ensuring effective protection of the system equipment. This protection scheme prevents the malfunction of protective devices unrelated to the fault location caused by the zero-sequence current flowing through the neutral line of Yg-D transformers in DG-connected systems.

With the growing complexity of future power systems, relying solely on simulation environments for developing protection strategies has limitations. Therefore, this paper verifies the proposed protection method in simulation and real-time HILS environments. Using HILS for protection coordination tests enables real-time monitoring of hardware test results and immediate analysis of the causes of protection coordination failures, facilitating prompt problem resolution through algorithm and firmware updates. Hence, despite the initial equipment costs, HILS can be a sustainable solution for developing innovative protection strategies from a long-term perspective.

Since the fault current decreases toward the end of the line in the system, in the Republic of Korea, different TCC curves are applied to each point in the system, or the pickup current is adjusted. However, this paper represents an initial research stage proposing a

protection method for the NDS based on the TCI curve. In other words, the optimization of protective device parameters was not considered, and the default parameter settings applied in the Republic of Korea were utilized. For the proposed method to be implemented in the real-world NDS, proper optimization of protective device parameters based on the locations of breakers is crucial. Accordingly, enhancing the accuracy of the operation of protective devices and contributing to system stability through internal parameters of the protective device optimization will be addressed in future research. The specific future research roadmap will deal with more sophisticated primary and backup protection in a wider range of scenarios than this paper after internal parameter optimization. In addition, various protection coordination problem scenarios and protection solutions occurring in recent systems will be studied. This study could include protection coordination issues depending on the number or location of connected DGs.

In summary, the NDS can be an effective solution in renewable energy policies, and the reliability of the power supply can become more important than before. However, the distribution line connected structure requires bidirectional fault current flows and an advanced protection method. Therefore, the proposed TCI-based protection method can selectively and quickly eliminate system faults and suggests the need for HILS, an advanced protection verification method. As a result, the proposed method is expected to be sustainably utilized in developing protective devices and more advanced protection coordination methods in the future.

Author Contributions: Conceptualization, J.N., W.C. and W.K.; data curation, J.N. and S.C.; formal analysis, J.N. and M.Y.; funding acquisition, S.C.; investigation, S.C.; methodology, J.N. and S.G.; project administration, W.C., W.K. and S.C.; resources, W.K.; software, J.N. and S.G.; supervision, S.C.; validation, J.N., S.G. and M.Y.; visualization, J.N. and S.C.; writing—original draft, J.N.; writing—review and editing, J.N. and S.C. All authors have read and agreed to the published version of the manuscript.

Funding: This research was supported in part by the Human Resources Program in Energy Technology of the Korea Institute of Energy Technology Evaluation and Planning (KETEP) and the Ministry of Trade, Industry & Energy (MOTIE) of the Republic of Korea (No. 20204010600220) and in part by the Korea Institute of Energy Technology Evaluation and Planning (KETEP) and the Ministry of Trade, Industry & Energy (MOTIE) of the Republic of Korea (No. 20225500000110).

Institutional Review Board Statement: Not applicable.

Informed Consent Statement: Not applicable.

Data Availability Statement: Not applicable.

Acknowledgments: The authors would like to thank Shin Sung Industrial Electric Corp. (SSIEC) Research Institute for technical support in using its protective devices in the HILS.

Conflicts of Interest: The authors declare no conflict of interest.

References

1. Guerrero, J.M.; Blaabjerg, F.; Zhelev, T.; Hemmes, K.; Monmasson, E.; Jemei, S.; Comech, M.P.; Granadino, R.; Frau, J.I. Distributed generation: Toward a new energy paradigm. *IEEE Ind. Electron. Mag.* **2010**, *4*, 52–64. [CrossRef]
2. Strachan, N.; Dowlatabadi, H. Distributed generation and distribution utilities. *Energy Policy* **2002**, *30*, 649–661. [CrossRef]
3. Roy; Kumar, N.; Pota, H.R. Current Status and Issues of Concern for the Integration of Distributed Generation into Electricity Networks. *IEEE Syst. J.* **2014**, *9*, 933–944. [CrossRef]
4. Hossain, E.; Tur, M.R.; Padmanaban, S.; Ay, S.; Khan, I. Analysis and Mitigation of Power Quality Issues in Distributed Generation Systems Using Custom Power Devices. *IEEE Access* **2018**, *6*, 16816–16833. [CrossRef]
5. Coster, E.J.; Myrzik, J.M.A.; Kruimer, B.; Kling, W.L. Integration Issues of Distributed Generation in Distribution Grids. *Proc. IEEE* **2010**, *99*, 28–39. [CrossRef]
6. Renders, B.; De Gussemé, K.; Ryckaert, W.R.; Vandevelde, L. Converter-connected distributed generation units with integrated harmonic voltage damping and harmonic current compensation function. *Electr. Power Syst. Res.* **2009**, *79*, 65–70. [CrossRef]
7. Kuang, H.; Li, S.; Wu, Z. Discussion on advantages and disadvantages of distributed generation connected to the grid. In Proceedings of the 2011 International Conference on Electrical and Control Engineering, Yichang, China, 16–18 September 2011; pp. 170–173.

8. Ismael, S.M.; Abdel Aleem, S.H.E.; Abdelaziz, A.Y.; Zobaa, A.F. State-of-the-art of hosting capacity in modern power systems with distributed generation. *Renew. Energy* **2019**, *130*, 1002–1020. [CrossRef]
9. Jacob; Anna, R.; Zhang, J. Distribution Network Reconfiguration to Increase Photovoltaic Hosting Capacity. In Proceedings of the 2020 IEEE Power & Energy Society General Meeting (PESGM), Montreal, QC, Canada, 2–6 August 2020; pp. 1–5.
10. Kolenc, M.; Papič, I.; Blažič, B. Assessment of maximum distributed generation penetration levels in low voltage networks using a probabilistic approach. *Int. J. Electr. Power Energy Syst.* **2015**, *64*, 505–515. [CrossRef]
11. Sakar, S.; Balci, M.E.; Abdel Aleem, S.H.A.; Zobaa, A.F. Increasing PV hosting capacity in distorted distribution systems using passive harmonic filtering. *Electr. Power Syst. Res.* **2017**, *148*, 74–86. [CrossRef]
12. Rahi, S.B.; Bisui, S.; Misra, S.C. Identifying critical challenges in the adoption of cloud-based services. *Int. J. Commun. Syst.* **2017**, *30*, e3261. [CrossRef]
13. Wiboonrat, M. Risk anatomy of data center power distribution systems. In Proceedings of the 2008 IEEE International Conference on Sustainable Energy Technologies, Singapore, 24–27 November 2008; pp. 674–679.
14. Shuai, M.; Chengzhi, W.; Shiwen, Y.; Hao, G.; Jufang, Y.; Hui, H. Review on economic loss assessment of power outages. *Procedia Comput. Sci.* **2018**, *130*, 1158–1163. [CrossRef]
15. Alvarez-Herault, M.-C.; N'doye, N.; Gandioli, C.; Hadjsaid, N.; Tixador, P. Meshed distribution network vs reinforcement to increase the distributed generation connection. *Sustain. Energy Grids Netw.* **2015**, *1*, 20–27. [CrossRef]
16. Davoudi, M.; Cecchi, V.; Agüero, J.R. Investigating the ability of meshed distribution systems to increase penetration levels of Distributed Generation. In Proceedings of the IEEE SOUTHEASTCON 2014, Lexington, KY, USA, 13–16 March 2014; pp. 1–5.
17. Celli, G.; Pilo, F.; Pisano GI UD IT, T.A.; Allegranza, V.; Cicoria, R.; Iaria, A. Meshed vs. radial MV distribution network in presence of large amount of DG. In Proceedings of the IEEE PES Power Systems Conference and Exposition 2004, New York, NY, USA, 10–13 October 2004; Volume 2, pp. 709–714.
18. Sharaf, H.M.; Zeineldin, H.H.; Ibrahim, D.K.; El Zahab EE, D.A. Protection coordination of directional overcurrent relays considering fault current direction. In Proceedings of the IEEE PES Innovative Smart Grid Technologies, Istanbul, Turkey, 12–15 October 2014; pp. 1–5.
19. Saleh, K.A.; Zeineldin, H.H.; Al-Hinai, A.; El-Saadany, E.F. Optimal coordination of directional overcurrent relays using a new time–current–voltage characteristic. *IEEE Trans. Power Deliv.* **2014**, *30*, 537–544. [CrossRef]
20. Zeineldin, H.H.; Sharaf, H.M.; Ibrahim, D.K.; El-Zahab, E.E.-D.A. Optimal Protection Coordination for Meshed Distribution Systems with DG Using Dual Setting Directional Over-Current Relays. *IEEE Trans. Smart Grid* **2014**, *6*, 115–123. [CrossRef]
21. Tsimtsios, A.M.; Korres, G.N.; Nikolaidis, V.C. A pilot-based distance protection scheme for meshed distribution systems with distributed generation. *Int. J. Electr. Power Energy Syst.* **2019**, *105*, 454–469. [CrossRef]
22. Cao, W.; Wu, J.; Jenkins, N.; Wang, C.; Green, T. Operating principle of Soft Open Points for electrical distribution network operation. *Appl. Energy* **2016**, *164*, 245–257. [CrossRef]
23. Gandioli, C.; Alvarez-Hérault, M.-C.; Tixador, P.; Hadjsaid, N.; Medina, D.-M.R. Innovative distribution networks planning integrating superconducting fault current limiters. *IEEE Trans. Appl. Supercond.* **2013**, *23*, 5603904. [CrossRef]
24. Bouchahdane, M.; Bouhadda, W.I.; Chikhi, B.; Eltom, A. Study and Testing of the Directional Phase Overcurrent Protection and the RCA's Impact on Its Performance and Directional Decision Making. In Proceedings of the 2022 7th International Conference on Environment Friendly Energies and Applications (EFEA), Bagatelle Moka MU, Mauritius, 14–16 December 2022; pp. 1–6.
25. Momoh, J.A.; Surender Reddy, S. Value of Hardware-In-Loop for experimenting microgrid performance system studies. In Proceedings of the 2016 IEEE PES PowerAfrica, Livingstone, Zambia, 28 June–3 July 2016; pp. 199–203.

Disclaimer/Publisher's Note: The statements, opinions and data contained in all publications are solely those of the individual author(s) and contributor(s) and not of MDPI and/or the editor(s). MDPI and/or the editor(s) disclaim responsibility for any injury to people or property resulting from any ideas, methods, instructions or products referred to in the content.